# A Novel Compact High Gain Wide-Band Log Periodic Dipole Array Antenna for Wireless Communication Systems

Islam M. Ibrahim[1] · Mohamed I. Ahmed[2] · Hala M. Abdelkader[3] · M. M. Elsherbini[1,3]

## Abstract

This paper implies a prototype for a broad-band log periodic dipole antenna (LPDA) with dimensions of $20 \times 40 \times 0.508$ mm$^3$ equipped with directors. The LPDA is based on Roger's RT5880 with $\varepsilon r = 2.2$. The 4-arms with alternative stubs constitute the LPDA, which is evenly spaced on both lines. At the substrate's back, the 50Ω main feeder line is placed on partial ground. The directors are also incorporated and studied in a regular matrix at a predetermined distance to improve gain, further reduce side lobes, and widen the frequency band. The performance of the antenna covers a wide spectrum of millimeter waves ranging from 26 up to 44 GHz. The realized gain for the antenna is 8.97, 11.96, 13.96, and 14.29 dB at 28 GHz, 35 GHz, 38 GHz, and 43 GHz, respectively. The total gain is 14.29 dB as a peak gain. The antenna was designed and tested for 5G communication applications in autonomous vehicles, and the design cost for the antenna is low in comparison to dielectric lenses. The model exhibits symmetrical radiation patterns for the antenna range. The results of the simulations and the testing of the implemented antenna elements coincide quite well. The proposed design outperforms earlier work in this field.

✉ M. M. Elsherbini
  motaz.ali@feng.bu.edu.eg

[1] Department of Electrical Engineering, The Egyptian Academy for Engineering and Advanced Technology (EAEAT), Cairo, Egypt

[2] Microstrip Department, Electronic Research Institute, El-Nuzha, Cairo 11843, Egypt

[3] Department of Electrical Engineering, Faculty of Engineering at Shoubra, Benha University, Cairo 11672, Egypt

# 1 Introduction

Antenna systems were developed to transport signals at a speedy rate with a lot higher capacity, thanks to antennas with a broad range and high gain as well as the quick development of communication technology. The suggested AVA is manufactured on RT 5880 and has the following dimensions: 30 mm × 12 mm × 0.5 mm. The deformations increase the gain of the simple Fermi-Dirac process AVA with a gain ranging from 7.2 to 13.1 dBi. A pair of components with two bands, 5G proposed to use MIMO antenna. The microstrip design has been engineered to function at the resonant frequencies of 26 to 30 GHz, 36 to 41.5 GHz, and beyond [1, 2]. An array antenna of 1 × 8 is created. The observed range is from 43 to 48 GHz, and the impedance spectrum of the array includes 14.8% between 41.9 and 48.6 GHz [3]. The planned AVA works in the micro and millimeter wave parts of the spectrum, spanning 2.6 GHz to the above 300 GHz. The AVA offers a consistent radiation pattern. The purpose of the "V"-shaped metamaterial is to increase gain [4]. The millimeter-wave antenna design process has exploded with the advancement of 5G networks, leading to the release of a range of MM-Wave antenna arrays. Since matching is essential for enhanced gain and spectrum, the Mmw is used to improve these systems. For a 5.8 GHz wireless local area network, an fr-4 substrate and an NZIM array configuration improves gain [5, 6]. Nevertheless, log periodic filters were employed to lessen the significant degradation in the Mm-wave bandwidths brought on by waves absorbing in the propagation channel. Dipole arrays are particularly important because of their greater range, greater gain, and consistent radiation [6]. These have been utilized in a number of smartphone platforms, such as base stations (BTS) and phased array antennas [7]. The notion is that the range of an LPDA array could be radically boosted by adding additional dipoles to it. Since the lowest frequency reacts to the longest dipole, a larger size is designed to increase the range toward the lower frequency [8]. LPDA antenna feeder techniques were also the focus of many studies. A recommended study on Mm-wave telecommunications bands around 24–28 GHz and 37–40 GHz maximizes the use of coaxial feed [9]. Patches are used to create a frequency that is lower than the outcomes from the first element. Using gap capacitive and capacitance, an extra resonance point is produced in accordance with the series resonance theory. It may also be viewed as a dimension decrease in order to reach a lower frequency range without needing a bigger total area [10]. A U-shaped slot with SIW LPDA is suggested at 28 GHz. Nevertheless, no built model is offered in these studies, and neither is the corresponding measurement data reported [11]. The 5 bent arms of the LPDA layout could be compared to a Rogers in LPDA design. The circular patch array for the wide spectrum LPDA for MMW is constructed and tested for 5G telecommunications at a frequency spectrum of 25–35.5 GHz [12, 13]. A prototype for an LPDA Microstrip covering a range of 28 GHz that is appropriate for 5G was created utilizing HFSS. The wide range actually caused the gain to decrease, but the frequency can be compressed to increase the gain [14]. A dipole strip

with periodic elements is used to create the Yagi-antennas in order to increase gain and line impedance. It is designed to operate at a frequency of 28–38 GHz [15]. An 11-element LPDA array with a total area of $90 \times 52$ mm$^2$ is built on a thin substrate. Between 2.75 and at 3.53 GHz, and at 4 and 6.2 GHz, were the antenna bands [16]. A dual-band single-fed circular polarized dielectric resonator antenna was created for dual-purpose communication, like GPS [17]. I-shaped slots are suggested for use in 5G MIMO antenna systems operating at sub-6 GHz. The antenna is designed with pairs of folded radiating petals, each of which has a base buried within a double layer of FR-4 substrate. The two layers are separated by a common ground plane [18]. Carrel's hypothesis served as the foundation for the design of a single-element antenna, which was then enhanced with a 50-microstrip feed-line with two orthogonal branches, primarily improving the broadside radiation pattern and diversity characteristics [19]. Narrow bandwidth and poor radiation efficiency are drawbacks of on-chip antennas. In order to develop high-performance on-chip antennas for millimeter-wave and terahertz integrated-circuit applications [20]. This led to the creation of a small, architecturally straightforward, wideband, and highly effective antenna for use in V-band communication devices. A standard circle patch is used to design the antenna, and it is then modified using a second fractal circular patch [21]. A revolutionary new 3-D shared aperture $3 \times 3$ matrix antenna-array for 5G wireless networks operating in the 26 GHz band. The radiation elements are hexagonal patches just above the general dielectric substrate and are activated by a metallic rod across 24.0–28.4 GHz [22]. It is suggested to use an ultra-wideband multiple-input multiple-output antenna based on a small coplanar waveguide method. A wide impedance bandwidth ranging from 3 to 11 GHz defines the design. The design is an ideal fit for portable electronics and ultra-wideband wireless communication systems [23]. It is a linear multiple-input multiple-output antenna system that has been scaled down for 5G applications that operates at 28 GHz and 24.8 GHz. The antenna can operate between 28 and 24.8 GHz with a 15 dB gain for each frequency and a bandwidth of 2.1 and 1.9 GHz [24]. The pattern is a shortened patch in the form of a bear. The ground is sotted to generate a broadsided directional radiation pattern, and the radiator is composed of two circular slots and one rectangular slot at the feet of the patch. The directional antenna dimensions are 7 by 7 by 0.254 mm$^3$, and its estimated bandwidth ranges between 0.86 and 1.08 GHz [25]. With an emphasis on graphene enabled antennas, absorbers, and sensors, this article offers an operational view of advanced graphene-based electromagnetic devices and analyzes the advantages and disadvantages of alternative design techniques [26]. Dual-band, eight-element, MIMO antenna in the shape of an H for use in sub-6 GHz (5G) smartphone applications. The parts are positioned on both sides of the substrate and are designed for the side edge frame of smartphones. Ensuring low mutual interaction between antenna elements [27]. The antenna operates between 1.173 and 1.210 THz at 1.19 THz, 1.270 and 1.320 THz at 1.3 GHz, and 1.368 to 1.346 THz at 1.3 GHz (at 1.4 GHz). The antenna is manufactured on silicon with a 20-micrometer thickness and a dielectric constant of

11.9. By varying the chemical potential in terms of the graphene, parameters of the antenna such as frequency, gain, and efficiency were adjusted [28]. This is a broadband, four-port (MIMO), S-shaped mmWave antenna with a frequency range of 25–39 GHz. The S-shape antenna has a single element dimension of 10 mm by 12 mm and a four-port MIMO configuration dimension of 24 mm by 24 mm by 0.25 mm. The gain obtained overall is 7.1 dBi [29]. A smart phone's dual broadband sub-6GHz (MIMO) antenna setup. The antenna is made out of FR4. There are eight antennas and feedings. The designs are $150 \times 75 \times 0.8$ mm and $150 \times 6 \times 0.8$ mm in size, respectively. At 3.5 and 5 GHz, the system resonated [30]. The following will be covered in this essay: "Antenna configuration and layout with no directors" is discussed in Section 2. Section 3 should present the antenna design with a director matrix. Section 4 should include the details on the parametric studies for LPDA. Section 5 should present the discussions and observations. Section 6 should cover the antenna performance as well as the radiation characteristics. Section 7 should include the conclusions.

## 2  Antenna Design Without Directors

The LPDA array is imprinted on the RT5880. The entire antenna size is $40 \times 20$ mm, including all the length of the feed. The metallic depth is $t = 0.035$ mm, the thickness of the substrate is $h = 0.508$ mm, of $\tan_\delta = 0.0009$, a relative permittivity of $\varepsilon_r = 2.2$. The bending arms provide the highest range while minimizing the total dimensions of the antenna. The reverse is meant by a partial ground plane to achieve UWB behavior. Partial ground planes are crucial. In essence, incomplete grounds release some of the substrate energy. The quality factor decreases as a result of the decreased energy storage in the substrates. The bandwidth increases as the Q factor falls. The geometrical factor is the proportion of each adjacent item's length to width at the headmost location, along with the dipole elements N as well as the spacing factor r. The largest array's length, L1, may be calculated from its lowest resonance frequency, fmin, and the spacing factor r, which determines how far apart the dipole components are from one another. The top and bottom viewpoints of an actual LPDA design having 4 bending arms but no directors are shown in Fig. 1a and b. The nth dipole element of the designed LPDA antenna has the following parameters: Ln, Wn, and Sn. The micro-strip feeder width is abbreviated as $W_f$. The feeding Zo was adjusted by the dipole array to be roughly 50 ohm to match the vector network analyzer's readings. It is important to determine the geometrical constant, the number of dipole elements N (the suggested LPDA element has N = 4 elements), and the separation factor r. The separation parameter is the spacing between relative dipole elements, while the geometric constant is represented as the proportion of the widths and lengths of the relative dipole elements. The 50-ohm feeding line covers a section of the ground plane at the substrate's backside. All of the dipole arms are arranged uniformly along a parallel microstrip transmission line on both sides of the substrate.

**Fig. 1  a** LPDA Array Schematic
Diagram without Directors with
50-Ω line feeding; top view; (**b**)
back view



(a)



(b)
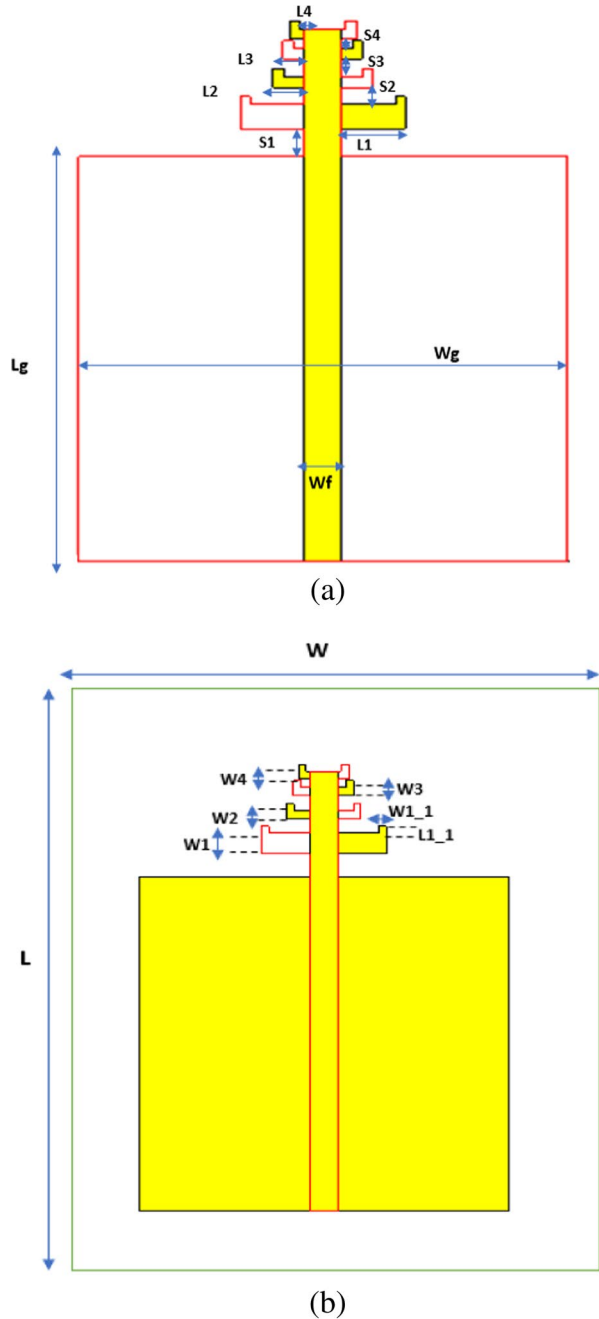
Antennas are designed using parameters such as dipole length Ln, width Wn, and the distance Sn between two dipoles. The other elements are calculated using the be-low-mentioned geometrical ratio once the length of the L1 has been established:

$$\tau = Ln/(L(n + 1)) = Sn/(S(n + 1)) = Wn/(W(n + 1)) = Fn/(F(n + 1)) \quad (1)$$

The spacing factor is defined as: where Fn+1 is bigger than fn and the parameter is:

$$\sigma = ((S(n + 1) - S(n))/(2L(n + 1))) \quad (2)$$

To find the LPDA number of dipole elements, we must use the following formula:

$$N = 1 + (Ln(Bs))/(Ln(1/\tau)) \quad (3)$$

According to the following formula, starting from the shortest (Lmin) element, the total length can be configured to the longest element (Lmax):

$$L = \lambda_{max}(1 - 1/Bs)\cot\alpha \quad (4)$$

$$\lambda max = 2Lmax = \frac{V}{fmin} \quad (5)$$

To ascertain the bandwidth of the active region (BAR), the following formula can be used to determine the effective dielectric constant $\varepsilon_{reff}$:

$$\varepsilon_{reff} = \left((\varepsilon_r + 1)/2\right) + \left((\varepsilon_r - 1)/2\right)1/\sqrt{\left(1 + 12h/W_1\right)} \quad (6)$$

$$Bs = B_{BAR} = B[1.1 + 7.7(1 - \tau2)\cot\alpha] \quad (7)$$

## 3 The Proposed LPDA Loaded with Directors

Along the y-axis, the directors' elements are stimulated. The optimum parameters for directors can be seen in Tables 1 and 2. It is possible to concentrate the current from the antenna through all these directors by forming the matrix of directors, which increases gain and decrease side lobes. To provide high performance for the array and enhance the high gain for the antenna, the directors were designed as microstrip patches in a circular shape and placed along the antenna at a y-axis on the front side at a parametrically studied distance from the antenna, beginning with 1 director and forming a row of them with a studied displacement between each director and each row. The effect of the director is shown in Table 3. We observe that the beam is focused forward as a result of the addition of directors. Directors will therefore improve the antenna's gain. They alter the radio waves' radiation patterns by re-radiating them with a new phase. As a result, "constructive interference" occurs, resulting in a stronger total signal and hence reducing the side lobes and enhancing the gain.

As stated, circular directors are advocated for the LPDA arrays. The same radiation effectiveness could well be reached because the current produced on the arms is more suitable for wave propagation than radiation. The first miniature LPDA is based on the arms shown in Fig. 2. The antenna with infused straight directors is

**Table 1** Dimensions of LPDA without Directors

| Symbol | Value (mm) |
|---|---|
| W | 20 |
| L | 40 |
| $W_f$ | 0.76 |
| $W_g$ | 10 |
| $L_g$ | 10.23 |
| L1 | 1.31 |
| L2 | 0.631 |
| L3 | 0.433 |
| L4 | 0.3 |
| W1 | 0.626 |
| W2 | 0.256 |
| W3 | 0.255 |
| W4 | 0.24 |
| S1 | 0.7 |
| S2 | 0.433 |
| S3 | 0.455 |
| S4 | 0.256 |
| L1_1 | 0.21 |
| W1_1 | 0.21 |
| h | 0.508 |

**Table 2** Optimized dimensions for directors

| Parameter | Value (mm) |
|---|---|
| r_Directors | 0.5 |
| Sp_Dir | 0.3 |
| $Sp_0$_ Dir | 0.506578 |
| W_ Dir | 11.40 |
| L_ Dir | 19.20 |
| d_ Dir | 1 |

equivalent to the unloaded antenna in Fig. 1, with the exception that the directors are contributed as a matrix in front of the antenna with fifteen concurrent straight rows to increase gain while also improving efficiency. For improved radiation and gain enrichment, the distance among director units and the diameter of the directors are also tuned. The directors are made to replace metamaterials and dielectric lenses in order to increase gain by producing a director's impact. Metamaterials inspire new ways of thinking about conventional electromagnetic ideas. The biggest downsides are the resonant properties of the metamaterial structures and some of the ensuing bandwidth restrictions. Antennas inspired by metamaterials often have low gain. The main difficulties are caused by the resonant properties of the metamaterial structures and certain resulting bandwidth restrictions. While metamaterials are the

| No. of Director | Realized gain(dB) |
|---|---|
| 1 Director | 11.47 |
| 3 Director | 11.64 |
| 5 Directors | 11.67 |
| (1 Row) contain (9) Directors | |
| 1 Row | 11.68 |
| 2 Row | 11.82 |
| 3 Row | 12.20 |
| 4 Row | 12.32 |
| 5 Row | 12.59 |
| 6 Row | 12.67 |
| 7 Row | 12.93 |
| 8 Row | 13.03 |
| 9 Row | 13.21 |
| 10 Row | 13.40 |
| 11 Row | 13.44 |
| 12 Row | 13.58 |
| 13 Row | 13.70 |
| 14 Row | 13.88 |
| 15 Row | 14.29 |

**Table 3** Realized gain values after studying the LPDA Directors

greatest candidates for 5G technologies, there are a few drawbacks that should be noted. (Metamaterials work over a restricted range of wavelengths, are challenging to create in large quantities, cannot change shape while operating, and are lossy. Our proposed work with directors outperforms metamaterial in terms of performance. [14].) The antenna configuration for dielectric lenses is heavy and large since lens antennas are used at low frequencies. For the same gain and bandwidth, these antennas cost more than reflector antennas for the same gain and bandwidth. The director's inclusion improves the antenna's range and impedance matching. The coupling between directors makes the spacing of the directors a significant element because it affects the reflection at the input. The spectrum and gain are drastically decreased with even a small amount of separation between directors. There will be substantial losses if the directors are too far apart.

## 4 Parametric Study

The directors are discretely incorporated in front of the antenna and are placed uniformly. The director, the reflectors, the dipole, and a section of the feeder line are imprinted on the upper layer of the substrate, as seen in Fig. 2. The gain in the antenna range increases only marginally when this configuration is modelled with a single set of directors placed far from the antenna at an optimal separation, with a 1.2 mm gap among directors. The gain was discovered to rise precisely at the highest frequency. Three additional directors were added. However,
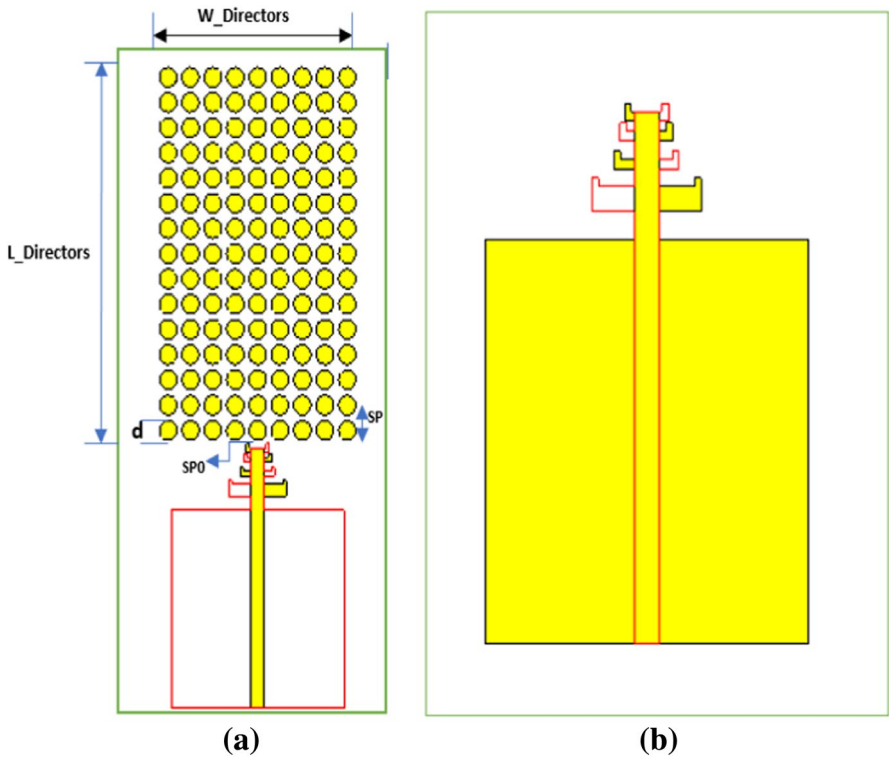
**Fig. 2** **a** LPDA Array Schematic Diagram with Directors; top view; (**b**) Back view

this had no good effects other than a slight increase in gain. As each row had nine items, the number of directors was extended by one row at a time. It created a 0.5 mm-diameter circle. The first row, which had an impact just on the antenna's gain, was indeed the subject of parametric research. On the basis of that,
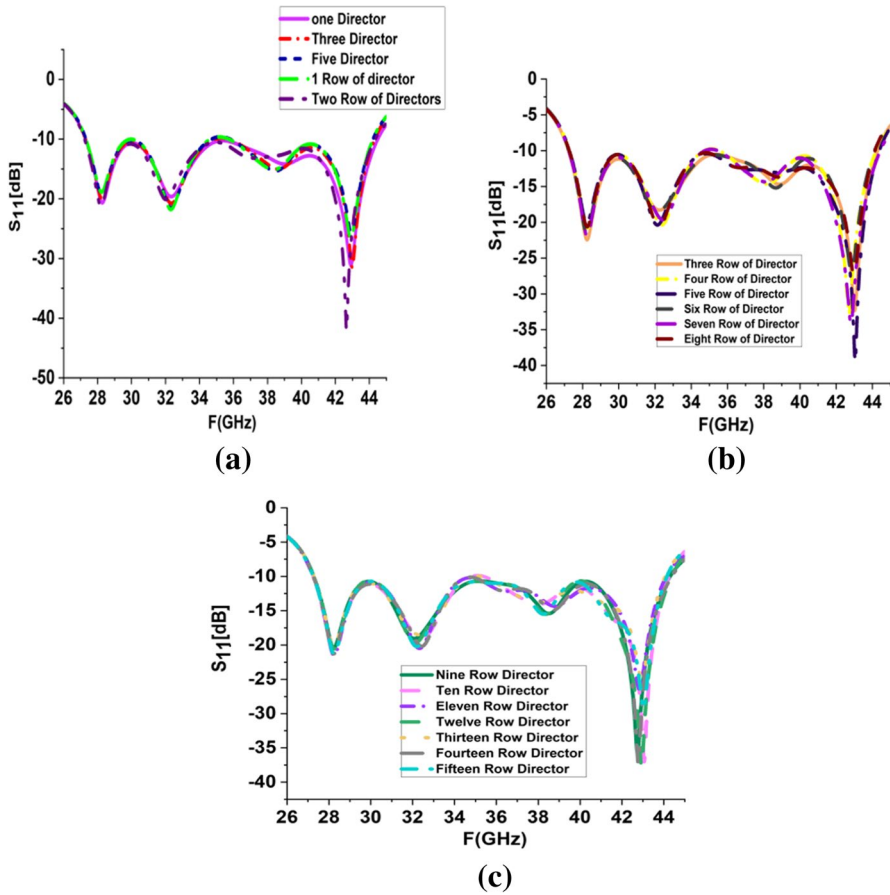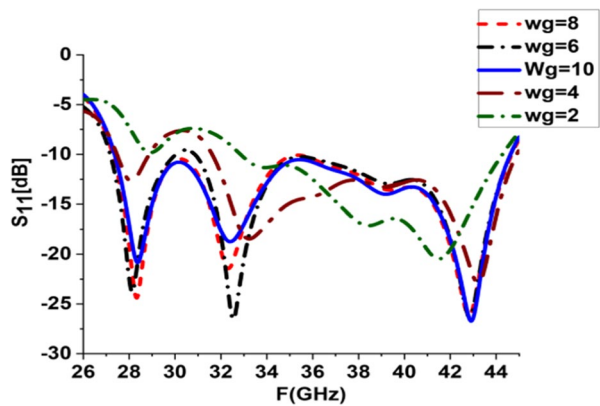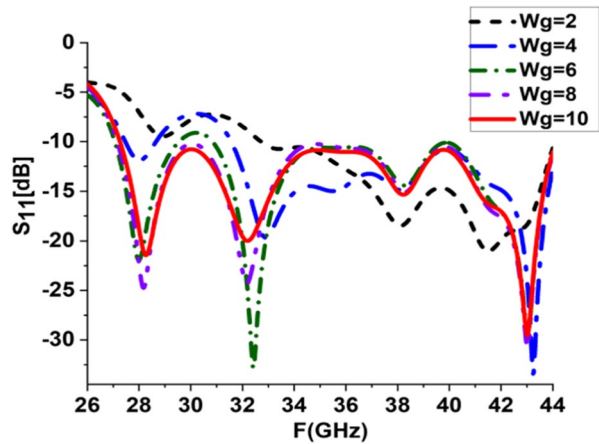
**Fig. 3** Chart for gain vs. increasing directors
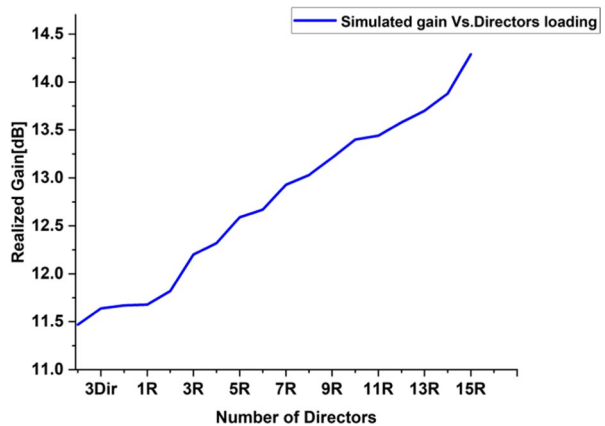
Fig. 4 (a), (b), (c) $S_{11}$ parametric study for increasing Directors numbers

Fig. 5 $S_{11}$ for simulated LDPA in $W_g$ without Directors

**Fig. 6** $S_{11}$ for simulated LDPA in $W_g$ with Directors



another row was added, and we discovered another rise in gain until there were 15 rows. After examining 15 rows, the gain began to progressively fall as the current concentration and energies fell, a reduction in the side lobe level (SLL), and an increase in the efficiency of the antenna. As a result, the maximum gain of the antenna is 14.29 dB, as depicted in Table 3 and Figs. 3. Additionally, there is a slight modification to $s_{11}$ in Figs. 4, 5 and 6. It is clear from the LPDA parameters that once the variable $W_g$ is changed, the side lobes of the recommended LPDA antenna must change to the $W_g$ parameter's best-optimized value. It ought to be clear that the parametric analysis led to the optimum $W_g$ value being set at 10 mm, as illustrated in Fig. 6. The performance of the antenna, particularly its radiation characteristics, is significantly impacted by the smaller ground width. Numerous parametric experiments were carried out using the MWSCST 2019 program to investigate the effects of a critical parameter, such

**Fig. 7** Total gain without dir. vs $W_g$
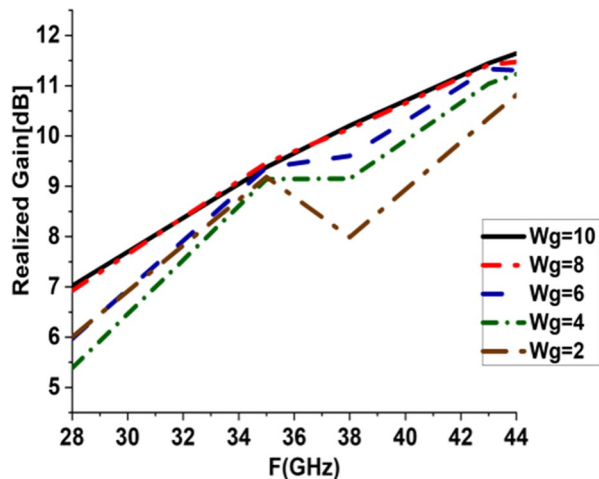
**Fig. 8** Total gain with dir. vs Wg
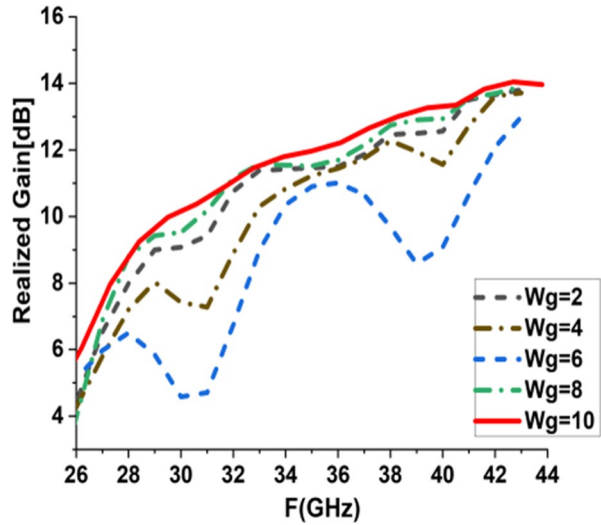


as the partial ground $W_g$, on the gain, bandwidth, and (SLL). By using built-in optimization methods within the CST, other variables can be enhanced and prepared for better matching bandwidth and high gain.

Figure 3 shows the curve or graph for increasing the directors' number step by step while the simulation process and parametric study for the directors, but Figs. 7, 8 and 9, shows the total realized gain for simulated and measured gain.
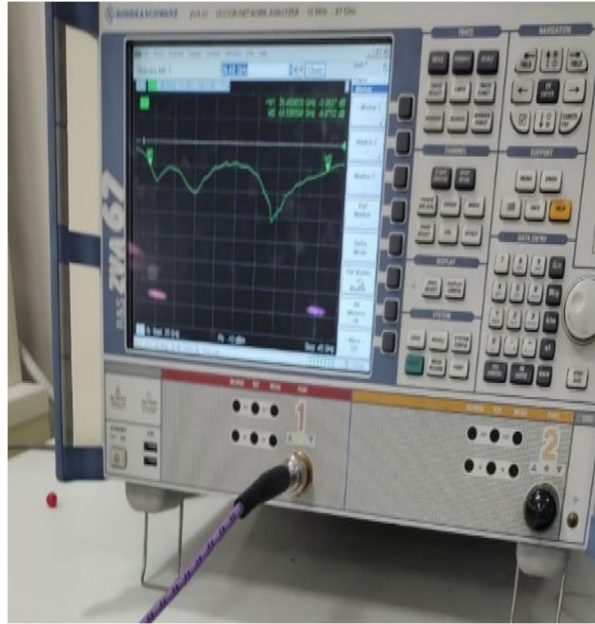
## 5 Results and Discussions

The $S_{11}$ of the built-in LPDA was measured using a Vector Network Analyzer ZVA 67 and a port impedance of 50 ohm. All test results are adjusted for the 50-ohm feeding line losses as shown in Fig. 10 and 11. Figure 12 compared the
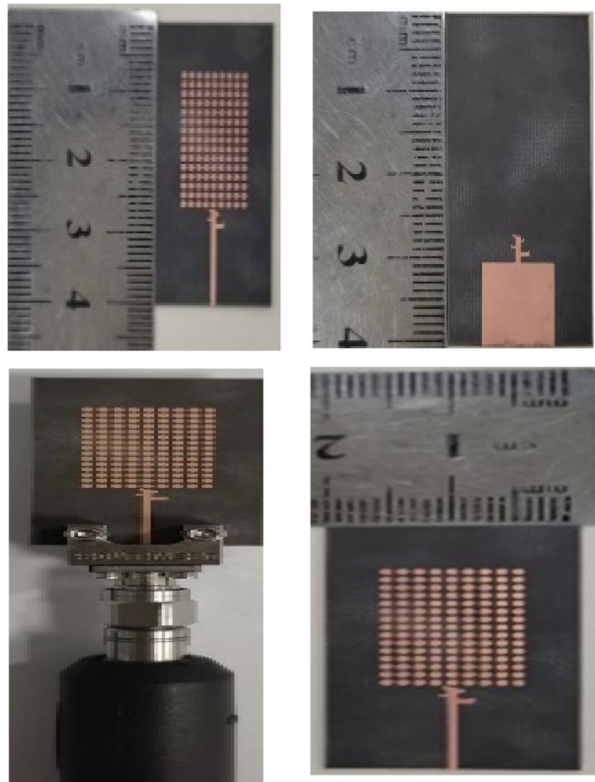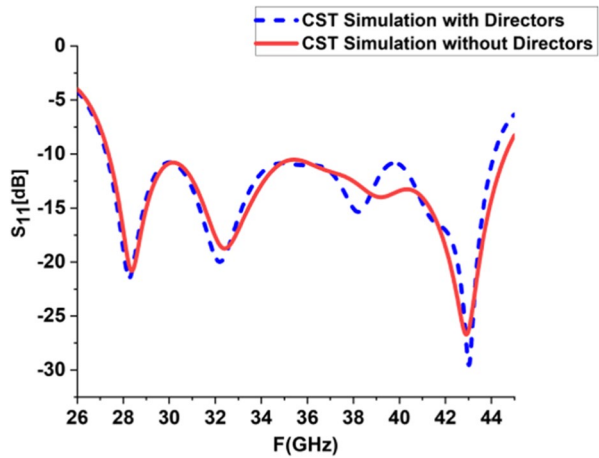
**Fig. 9** LPDA Total Realized gain
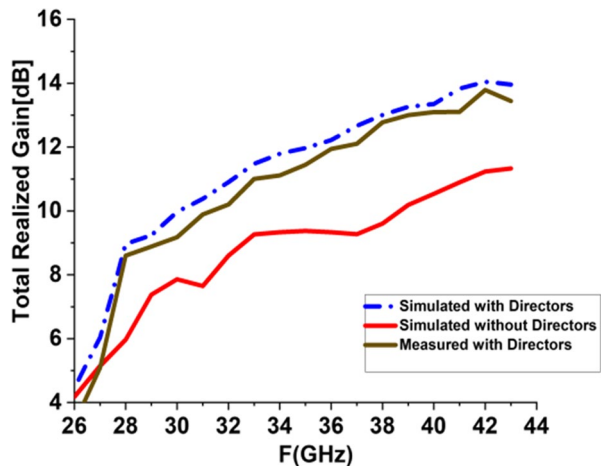
**Fig. 10** Photograph of the practical LPDA prototype antenna S-parameters measurements



**Fig. 11** Photograph of the Fabricated LPDA model

**Fig. 12** $S_{11}$ for LDPA with and without directors



outcomes of the simulation with and without directors to the observed $S_{11}$ up to 43 GHz. The test findings show that the antennas conform well and operate for 5G operations in a broad frequency range, between 26 and 44 GHz, with an $S_{11}$ below −10 dB as seen in Fig. 13. The proposed model has a measured $S_{11}$ of around −36.48 dB at 43 GHz compared to the modelling results of the MWSCST software, which were −28.99 dB. Simulation models typically produce consistent outcomes. The inconsistency in observed results is brought on by fabrication accuracy and the frequency-dependent permittivity behaviour of the substrate at higher frequencies, which could not be reliably simulated. In Fig. 12, in comparison to the LPDA without it, the simulation result of the scheme with directors exhibits the best result. Furthermore, the impedance frequency band has S-parameters ranging from 26 to 44 GHz. The overall gain from choosing to use fabrication to experimentally validate the simulations.

**Fig. 13** $S_{11}$ for simulated and measured LDPA with Directors
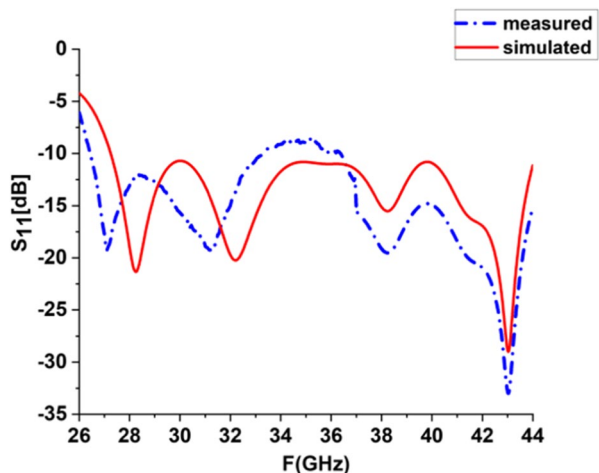
| Table 4 The impact of $W_g$ without directors on $S_{11}$ | Wg | $S_{11}$ (dB) | Total gain (dB) |
|---|---|---|---|
| | 2 | − 20.459 | 11.31 |
| | 4 | − 22.908 | 11.01 |
| | 6 | − 26.55 | 11.16 |
| | 8 | − 26.162 | 11.32 |
| | 10 | − 26.716 | 11.48 |

Furthermore, the gain is improved and raised to 14.29 dB at 43 GHz with full directors. The antenna clearly covers a broad frequency range with S11 around −26.95 dB, with antenna performance spanning from 26 to 44 GHz. It is clear from Fig. 13 that the S-parameter only slightly changes, but the gain rises due to the directors' presence and the surface current that passes through them, lowering loss. It was discovered that the $S_{11}$ value had reached about −28.99 dB.

When the director's matrix was incorporated into the design, as illustrated in Fig. 4, it was noticed that the S-parameter in the parametric studies had slightly changed. However, it was found that by altering the value of the variable Wg in the presence and absence of directors, the best choice was found to be 10 mm, as seen in Figs. 5 and 6. Also, Tables 4 and 5 show the numerical values for the total gain and $S_{11}$ resulting from the intensive parametric study for the chosen convenient value for $W_g$.

## 6 Antenna Gain and Radiation Pattern Measurements

The gain of LPDA was calculated using the radiation pattern measurements. Two consecutive and equivalent horn antennas that were put up in an aligning configuration that was line-of-sight at a separation of R were used to determine the gain. While another is used for receiving, the first is utilized for transmitting. They must be separated by a distance greater than or equal to $R = 2D^2/\lambda_O$, where D and $\lambda_O$ are the antenna's greatest aperture dimensions and the wavelength for free-space at the operating frequency f, in order to satisfy the far-field requirement.

| Table 5 $S_{11}$ with the impact of directors on Wg | Wg | $S_{11}$ (dB) | Total gain (dB) |
|---|---|---|---|
| | 2 | − 21.439 | 12.59 |
| | 4 | − 28.15 | 13 |
| | 6 | − 26.97 | 12.97 |
| | 8 | − 25.428 | 11.32 |
| | 10 | − 29.98 | 14.29 |

$$Pr/Pt = |S21|^2 = GtGr(\lambda_O/4\pi R)^2 \tag{8}$$

Power sent and received are denoted by $P_t$ and $P_r$, respectively. Due to the similarities of the two antennas, the observed transmission coefficient from the VNA is represented by the power ratio Pr/Pt. within Fig. 9. The simulation's results indicate improved concordance between both the simulated and measured gains. The antenna's total gain has been calculated to be 14.29 GHz at 43 GHz, 13.44 GHz at 38 GHz, 11.44 dBi at 35 GHz, and 8.60 GHz as shown in Tables 6 . Since the accuracy of the measurement equipment diminishes with frequency, there is a mismatch between what was modelled and what was measured. Scattering and reflection from the environment also contribute to this. Prior to measurements, there was no absorbent material covering the Antenna under test (AUT). However, the total realized gain without directors has almost reached 11.48 dB with the best value for Wg in Fig. 7. It is evident that the LPDA gain has increased by about 3 dB overall.

An AUT is installed on a revolving surface and rotated around at an azimuth to produce a 2D pattern. The antenna's two primary axes are frequently measured to obtain details such as the beam's breadth in the H and E planes in Figs. 14 . A 360-degree rotating rod is installed for attaching the antenna under test. A second pole with the regular transmitting horn antenna attached to it is situated about 20 cm away. Multiple data sets must be acquired every 5° throughout time to measure the radiation pattern. This suggested configuration is used to plot the actual radiation patterns of the implemented antenna. Figs. 15 and 16 shows the modelled and measured radiation patterns of the antenna in the E-plane and H-plane at 28, 35, and 38 GHz. It is evident that the suggested antenna produces a consistent radiation pattern over the reported bandwidth. The radiation patterns in the H-plane and E-plane are depicted in Figs. 17 and 18, where better side-lobe suppression is demonstrated by the proposed LPDA antenna.

The director's matrix, which improves and enhances the high gain and stable radiation pattern antenna used for 5G applications, also covers a broadband range and wide bandwidth. The antenna also has better efficiency. The antenna has small dimensions, and the design cost for the antenna is low in comparison to dielectric lenses. Our proposed work has the highest gain compared to the previous work. This is the novelty and contribution of this work compared with previous works as shown in  Table 7.

| Table 6 Simulated and measured LPDA realized gain | Frequencies (GHz) | Simulated gain (dBi) | Measured gain (dBi) |
|---|---|---|---|
| | 28 | 8.97 | 8.60 |
| | 35 | 11.96 | 11.44 |
| | 38 | 13.96 | 13.44 |
| | 43 | 14.29 | 13.98 |

**Table 7** Comparison between proposed antenna and previous work

| Reference no | Frequency band (GHz) | Substrate | Overall gain (dBi) | No. of arms | Dimensions (mm) | Fabrication technology | Bandwidth (GHz) | Impedance bandwidth (%) | Design complexity |
|---|---|---|---|---|---|---|---|---|---|
| [13] | 25–45 | Rogers3003[R] | 10 | 3 | 150×75 | PCB | 20 | 57 | Complex |
| [14] | 26–39 | RO5880 | 11 | 5 | 25×10 | PCB | 13 | 40 | Complex |
| [19] | 12–22 | RT5880 | 4.2–10.7 | 8 | 35×20 | PCB | 10 | 58 | Complex |
| [21] | 55–75 | Duroid 5880 | 10.3 | Patch | 13×12 | PCB | 20 | 30 | Medium |
| [29] | 25–39 | RO5880 | 7.1 | 4- element | 24×24 | PCB | 14 | 43 | Complex |
| [39] | 25–35.5 | Arlon di clad 880TM | 11 | 5 | 20×38 | PCB | 10.5 | 34.73 | Simple |
| [48] | 28–38 | RO3003[TM] | 5.86 | 2 -element | 7.5×8.8 | PCB | 10 | 30 | Medium |
| [49] | 22–37 | RT5880 | 13.3 | 4 | 40×13 | PCB | 15 | 50 | Simple |
| Proposed work | 26–44 | RogersRT5880 | 14.29 | 4 | 20×40 | PCB | 18 | 51.5% | Simple |

**Fig. 14** LPDA radiation efficiency
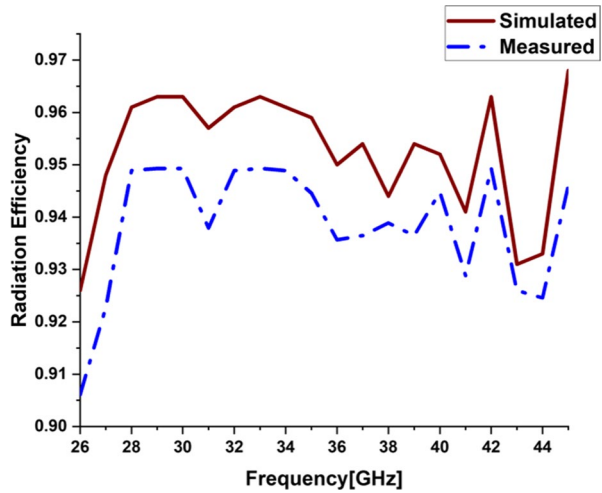


**Fig. 15** Schematic diagram for measurements setup
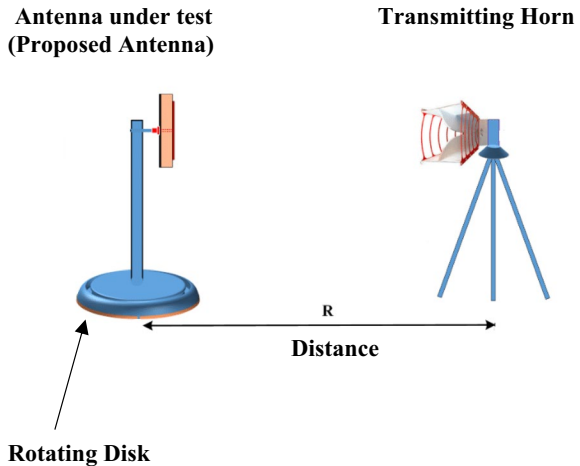


## 7 Conclusions

In this paper, a millimeter-wave functioning LPDA antenna was proposed. The wideband performance of the suggested architecture spans frequencies of 26 GHz to well over 45 GHz. At 43 GHz, the LPDA attained a total realized peak gain of 14.29 dBi. The LPDA enriches the gain at 28 GHz, 35 GHz, 38 GHz, and 43 GHz by 8.97 dB, 11.96 dB, 13.96 dB, and 14.29 dB, respectively. The antenna achieved a better efficiency of 96%. The impedance match for the array is nearly 52%. The proposed directors improved the bandwidth while also increasing the gain and antenna efficiency. The proposed antenna's radiation pattern and realized gain are simulated and measured. Numerous benefits, including a high antenna measured gain, wide band, a consistent radiation pattern, and good SLLs, are

**Fig. 16** Radiation pattern measurements setup





(a)E-plane 28GHz                (b) E-plane 35GHz                (c) E-plane 38GHz
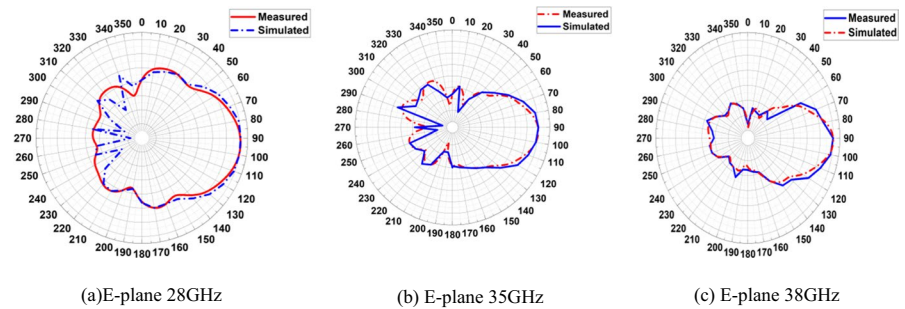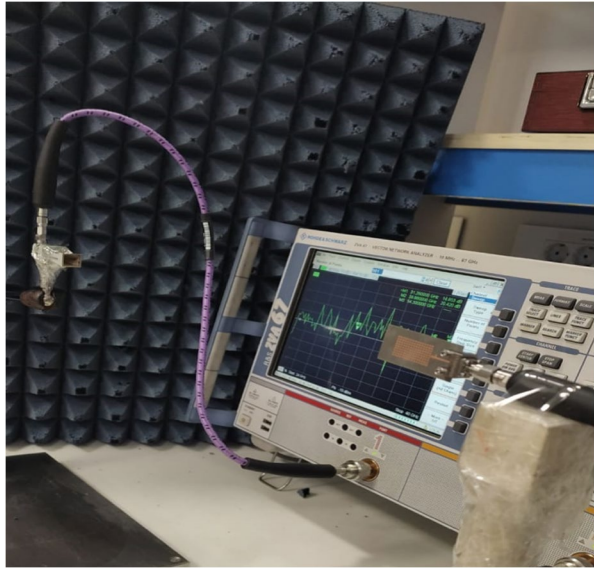
**Fig. 17** Simulated vs. Measured Radiation pattern of LPDA E-Plane at: (**a**) 28 GHz, (**b**) 35 GHz, (**c**) 38 GHz



(a) H-plane 28GHz                (b) H-plane 35GHz                (c) H-plane 38GHz
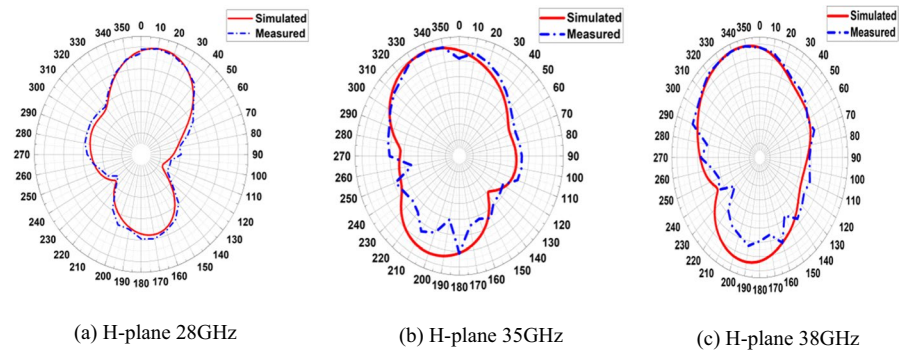
**Fig. 18** Simulated vs. Measured Radiation pattern of LPDA H-Plane at: (**a**) 28 GHz, (**b**) 35 GHz, (**c**) 38 GHz

confirmed by simulation using MWSCST software. According to simulated and measured data, the prototype antenna exhibits better properties than the current antennas in the literature. We claim that the proposed LPDA is one of the viable options for use in 5G autonomous vehicle applications.

**Author contribution** Mohamed I. Ahmed and M. M. Elsherbini wrote the main manuscript text; Islam M. Ibrahim and Mohamed I. Ahmed prepared figures. All authors reviewed the manuscript.

## Declarations

**Competing interests** The authors declare no competing interests.

## References

1. A.S. Dixit, S. Kumar, A Fermi-Dirac Function-based antipodal vivaldi antenna for mm wave applications, J Infrared Milli Terahz Waves, 43, 244–259,2022, https://doi.org/10.1007/s10762-022-00854-6
2. A.R. Sabek, W.A.E. Ali, & A.A. Ibrahim, Minimally coupled two-element MIMO antenna with dual band (28/38 GHz) for 5G wireless communications, J Infrared Milli Terahz Waves, 43, 335–348 ,2022, https://doi.org/10.1007/s10762-022-00857-3
3. J. Xiao, T. Ding, D. Luo, et al. Circularly polarized antenna array using metallic slanted cross slot for 5G MMW applications, J Infrared Milli Terahz Waves ,43, 165–180, (2022), https://doi.org/10.1007/s10762-021-00837-z
4. S. Kumar, A.S. Dixit, Wideband antipodal vivaldi antenna using metamaterial for micrometer and millimeter wave applications. J Infrared Milli Terahz Waves 42, 974–985, (2021), https://doi.org/10.1007/s10762-021-00799-2
5. W.C. Weng, M.C. Chang, Ultra-wideband planar log-periodic slot antenna with exponential shapes on slot edges, The Applied Computational Electromagnetics Society Journal (ACES), Sep 1:1280–6, 2019
6. A. Khairy, I. Mohammed, M. I. Ahmed, & M. M. Elsherbini, The design of a superstate NZIM-antenna array for WLAN application, Journal of Engineering Advancements, 3(03), 72–75, (2022), https://doi.org/10.38032/jea.2022.03.001.
7. R. Eid, A. Elboushi, M. Hindy, Wideband monopole antenna with multiple stub resonators for 5G applications,38th National Radio Science Conference (NRSC), (Vol. 1, pp. 80–87), 2021 Jul 27, https://doi.org/10.1109/NRSC52299.2021.9509812.
8. H. Kawakami, M. Tanioka, R. Wakabayashi, Circularly polarized log periodic dipole antennas, International Applied Computational Electromagnetics Society Symposium (ACES), (pp. 1–2), 2020 Jul 27, https://doi.org/10.23919/ACES49320.2020.9196090

9.  M.A. Islam, H.M. Jihad, M.A. Muminin, N. Dhar, A. Begum, Design and simulation of a compact log periodic dipole array (LPDA) antenna for UWB applications, In2021 2nd International Conference for Emerging Technology (INCET), (pp. 1–5), 2021 May 21, https://doi.org/10.1109/INCET51464.2021.9456212.

10. O.M. Haraz, Millimeter-wave printed dipole array antenna loaded with a low-cost dielectric lens for high-gain applications, Journal of Infrared, Millimeter, and Terahertz Waves, (3):225–44. 2020 Mar,41, https://doi.org/10.1007/s10762-019-00654-5.

11. S.H. Kiani, X.C. Ren, A. Bashir, A. Rafiq, M.R. Anjum, M.M. Kamal, B.U. Din, F. Muhammad, Square-framed T shape mm wave antenna array at 28 GHz for future 5G devices, International Journal of Antennas and Propagation, 13,2021. 2021 Sep, https://doi.org/10.1155/2021/2286011.

12. S.M. Hamza, H. Ullah, F.A. Tahir, A miniaturized printed UWB LPDA antenna, In 2020 International Conference on UK-China Emerging Technologies (UCET), (pp. 1–3), 2020 Aug 20, https://doi.org/10.1109/UCET51115.2020.9205322

13. A. E. Farahat, & K.F.A. Hussein, Dual-band (28/38 GHz) Yagi–Uda antenna with corrugated radiator and triangular reflectors for 5G mobile phones, The Applied Computational Electromagnetics Society Journal (ACES), 36(10), 1325–1334, 2020 Aug, https://doi.org/10.13052/2021.ACES.J.361009.

14. R.E. Shehata, A. Elboushi, M. Hindy, H. Elmekati, Metamaterial inspired LPDA MIMO array for upper band 5G applications, International Journal of RF and Microwave Computer-Aided Engineering, e23212, 2022 May 2, https://doi.org/10.1002/mmce.23212.

15. R. Kubacki, M. Krzyzewski, D. Laskowski, Enlarged frequency bandwidth of truncated log-periodic dipole array antenna, Electronics, 13,9(8):1300, 2020 Aug, https://doi.org/10.3390/electronics9081300.

16. C. Peixeiro, Design of log-periodic dipole antennas, IEE Proceedings H (Microwaves, Antennas and Propagation), (Vol. 135, No. 2, pp. 98–102),1988 Apr 1, https://doi.org/10.1109/IRECON.1961.1151016.

17. J. Iqbal, U. Illahi, M.A. Khan, A. Rauf, E.M. Ali, I. Bari I, H. Ali, M.A. Khan, M. Alibakhshikenari, M. Dalarsson, A novel single-fed dual-band dual-circularly polarized dielectric resonator antenna for 5G sub-6GHz applications, Applied Sciences, 21;12(10):5222,2022 May, https://doi.org/10.3390/app12105222.

18. M. Alibakhshikenari, B.S. Virdee , C.H. See, P. Shukla, S.M. Moghaddam, A.U. Zaman, S. Shafqaat, M.O. Akinsolu, B. Liu, J. Yang, R. Abd-Alhameed, Dual-polarized highly folded bowtie antenna with slotted self-grounded structure for sub-6 GHz 5G applications, IEEE Transactions on Antennas and Propagation.;70(4):3028-33., 2021 Oct 14, https://doi.org/10.1109/TAP.2021.3118784.

19. M.M. Fakharian, M. Alibakhshikenari, C.H. See, R. Abd-Alhameed, A high gain multiband offset MIMO antenna based on a planar log-periodic array for Ku/K-band applications, Scientific Reports, 8;12(1):1–3, 2022 Mar, https://doi.org/10.1038/s41598-022-07866-1.

20. M. Alibakhshikenari, E.M. Ali, M. Soruri , M. Dalarsson , M. Naser-Moghadasi , B.S. Virdee , C. Stefanovic , A. Pietrenko-Dabrowska , S. Koziel , S. Szczepanski ,E. Limiti, A comprehensive survey on antennas on-chip based on metamaterial, metasurface, and substrate integrated waveguide principles for millimeter-waves and terahertz integrated circuits and systems, IEEE Access.,. IEEE Access, vol. 10, pp. 3668–3692, 2022, https://doi.org/10.1109/ACCESS.2021.3140156.

21. M. Hussain, S.I. Naqvi, W.A. Awan, W.A. Ali, E.M. Ali, S. Khan, M. Alibakhshikenari, Simple wideband extended aperture antenna-inspired circular patch for V-band communication systems, AEU-International Journal of Electronics and Communications,144:154061, 2022 Feb 1, https://doi.org/10.1016/j.aeue.2021.154061.

22. M. Alibakhshikenari, B.S. Virdee, V. Vadalà, M. Dalarsson, M.E. de Cos Gómez, A.G. Alharbi, S.N. Burokur, S. Aïssa, I. Dayoub, F. Falcone, E. Limiti, Broadband 3-D shared aperture high isolation nine-element antenna array for on-demand millimeter-wave 5G applications, Optik,267:169708. 2022 Oct 1, https://doi.org/10.1016/j.ijleo.2022.169708.

23. S. Ahmad, S. Khan, B. Manzoor, M. Soruri, M. Alibakhshikenari, M. Dalarsson, F. Falcone, A compact CPW-fed ultra-wideband multi-input-multi-output (MIMO) antenna for wireless communication networks, IEEE Access,10:25278-89., 2022 Mar 2, https://doi.org/10.1109/ACCESS.2022.3155762.

24. W.A. Awan, M. Soruri, M. Alibakhshikenari, E. Limiti, On-demand frequency switchable antenna array operating at 24.8 and 28GHz for 5G high-gain sensors applications, Progress in Electromagnetics Research M, Vol. 108, 163–173, 2022, https://doi.org/10.2528/PIERM21121102.

25. S. Ahmad, B. Manzoor, K.N. Paracha, S. Haider, M. Liaqat, A.J. Al-Gburi, A. Ghaffar, M. Alibakhshikenari, M. Dalarsson, A wideband bear-shaped compact size implantable antenna for in-body communications, Applied Sciences,12(6): 2859, 2022 Mar 10, https://doi.org/10.3390/app12062859.

26. M. Esfandiari, A. Lalbakhsh, P.N. Shehni, S. Jarchi, M. Ghaffari-Miab, H.N Mahtaj, S. Reisenfeld, M. Alibakhshikenari, S. Koziel, S. Szczepanski, Recent and emerging applications of

graphene-based metamaterials in electromagnetics. Materials & Design, 110920.Materials & Design, Volume 221, 110920, 2022 Jul 6, https://doi.org/10.1016/j.matdes.2022.110920.

27. M.N. Zahid, Z. Gaofeng, S.H. Kiani, U. Rafique, S.M. Abbas, M. Alibakhshikenari, M. Dalarsson, H-shaped eight-element dual-band MIMO antenna for sub-6 GHz 5G smartphone applications, IEEE Access, vol. 10, pp. 85619-85629, 2022, https://doi.org/10.1109/ACCESS.2022.3189658.

28. I.E. Lamri, S. Ahmad, M.F. Nakmouche, A. Ghaffar, D.E. Fawzy, A.M Allam, E.M. Ali, M. Dalarsson, M. Alibakhshikenari, Design and development of a graphene-based reconfigurable patch antenna array for THz applications. Frequenz.,2022 Jul 11, https://doi.org/10.1515/freq-2022-0051.

29. M.A. Khan, A.G. Al Harbi, S.H. Kiani, A.N. Nordin, M.E. Munir, S.I. Saeed, J. Iqbal, E.M. Ali, M. Alibakhshikenari, M. Dalarsson, mm Wave four-element MIMO antenna for future 5G systems, Applied Sciences,12(9):4280, 2022 Apr 23, https://doi.org/10.3390/app12094280.

30. S.H. Kiani, A. Iqbal, S.W. Wong, H.S. Savci, M. Alibakhshikenari, M. Dalarsson, Multiple elements MIMO antenna system with broadband operation for 5th generation smart phones, vol. 10, pp. 38446–38457, 2022 Apr 5, https://doi.org/10.1109/ACCESS.2022.3165049.

31. Q.X. Chu, X.R. Li, M. Ye, High-gain printed log-periodic dipole array antenna with parasitic cell for 5G communication. IEEE Transactions on Antennas and Propagation,65(12):6338-44. 2017 Jul 6. https://doi.org/10.1109/TAP.2017.2723916.

32. S. Yang, H. Zhai, J.Li, Y. Zeng, A new printed log-periodic dipole array (PLPDA) antenna with bandwidth broadening and gain improving. International Journal of RF and Microwave Computer Aided Engineering, e22266. 2020 Aug;30. https://doi.org/10.1002/mmce.22266.

33. A. Talbi, M. Nedil, Millimeter-wave SIW cavity-backed dual-band self-complementary log-periodic antenna. In 2019 IEEE International Symposium on Antennas and Propagation and USNC-URSI Radio Science Meeting, (pp. 1125–1126). 2019 Jul 7 https://doi.org/10.1109/APUSNCURSINRSM.2019.8888360.

34. T. Sepdiansah, Y. Mukhlis, M.F. Salam, A printed log-periodic dipole array (LPDA) antenna for 5G application. In 2019 Fourth International Conference on Informatics and Computing (ICIC), (pp. 1–5). 2019 Oct 16. https://doi.org/10.1109/ICIC47613.2019.8985792.

35. K.K. Mistry, P.I. Lazaridis, T.H. Loh, Z.D. Zaharis, I.A. Glover, B. Liu, A novel design of a 10-dipole log-periodic antenna with LTE-800 and GSM-900 band rejection. In 2019 IEEE MTT-S International Conference on Numerical Electromagnetic and Multiphysics Modeling and Optimization (NEMO), (pp. 1–4). 2019 May 29. https://doi.org/10.1109/NEMO.2019.8853709.

36. M.E. Munir, A.G. Al Harbi, S.H. Kiani, M. Marey, N.O. Parchin, J. Khan, H. Mostafa, J. Iqbal, M.A. Khan, C.H. See, R.A. Abd-Alhameed, A new mm-wave antenna array with wideband characteristics for next generation communication systems. Electronics,11(10). 15602022 May 13. https://doi.org/10.3390/electronics11101560.

37. A.E. Farahat, K.F. Hussein, 28/38 GHz dual-band Yagi-Uda antenna with corrugated radiator and enhanced reflectors for 5G MIMO antenna systems. Progress In Electromagnetics Research C, 101:159-72. 2020. https://doi.org/10.2528/PIERC20022603

38. H. Abutarboush, O.F. Siddiqui, M.R. Wali, F.A. Tahir, A highly bendable log-periodic array antenna for flexible electronics. Progress In Electromagnetics Research M, 96:99–107. 2020.https://doi.org/10.2528/PIERM20071402

39. V. Harini, M.V. Sairam, R.A. Madhu, Wide band log periodic millimeter-wave antenna for 5G femtocells applications. Transactions on Emerging Telecommunications Technologies, .1;32(11). 2021 Nov. https://doi.org/10.1002/ett.4321.

40. A. Ahmad, D.Y. Choi, S. Ullah, A compact two elements MIMO antenna for 5G communication. Scientific Reports,12(1):1-8. 2022 Mar 4. https://doi.org/10.1038/s41598-022-07579-5.

41. Y. Luo, Y. Shen, X. Cai, F. Qian, S. Xu, H. Cui, G. Yang, Substrate integrated coaxial line design for mm Wave antenna with multilayer configuration. International Journal of RF and Microwave Computer Aided Engineering,32(5): e23090. 2022 May. https://doi.org/10.1002/mmce.23090.

42. U. Farooq, G.M. Rather, A miniaturized Ka/V dual band millimeter wave antenna for 5G body centric network applications. Alexandria Engineering Journal, 2022 Oct 1;61(10):8089-96. https://doi.org/10.1016/j.aej.2022.01.044.

43. J. Khan, S. Ullah, U. Ali, F.A. Tahir, I. Peter, L. Matekovits, Design of a millimeter-wave MIMO antenna array for 5G communication terminals. Sensors, 22(7):2768. 2022 Apr 4. https://doi.org/10.3390/s22072768.

44. O.A. Shareef, A.M. Sabaawi, K.S. Muttair, M.F. Mosleh, M.B. Almashhdany, Design of multi-band millimeter wave antenna for 5G smartphones. Indonesian Journal of Electrical Engineering and Computer Science,25(1):382–7. 2022 Jan. https://doi.org/10.11591/ijeecs.v25.i1.pp382-387.

45. H. Wang, H. Wu, B. Li, H. Qin, Miniaturization design of log periodic dipole antenna based on dovetail structure. International Journal of RF and Microwave Computer-Aided Engineering, e23263.2022. https://doi.org/10.1002/mmce.23263.
46. P. Sari, A. Firdausi, G.P. Hakim, The design of log periodic dipole array microstrip antenna at frequency 28 GHz. In 2020 2nd International Conference on Broadband Communications, Wireless Sensors and Powering (BCWSPx, (pp. 140–143).) 2020 Sep 28 https://doi.org/10.1109/BCWSP 50066.2020.9249467.
47. C.A. Balanis, Antenna theory, analysis and design John Wiley & Sons, 2015 Dec 28.
48. A.E. Farahat, K.F. Hussein, Dual-band (28/38 GHz) wideband MIMO antenna for 5G mobile applications. IEEE Access, 2022 Mar 21, 10:32213-23. https://doi.org/10.1109/ACCESS.2022.316072.
49. A. Mahabub, S.M. Sifat, A.A. Kishk, High gain wideband log-periodic antenna with directors and perforation for 5G application. In 2020 IEEE USNC-CNC-URSI North American Radio Science Meeting (Joint with AP-S Symposium), (pp. 53–54). 2020 Jul 5 https://doi.org/10.23919/USNC/ URSI49741.2020.9321690.